A study on incorporation of thermoelectric modules with evacuated-tube heat-pipe solar collectors

Wei He [a,*], Yuehong Su [b], Y.Q. Wang [a], S.B. Riffat [b], Jie Ji [a]

[a] Department of Thermal Science and Energy Engineering, University of Science and Technology of China, No.96 Jinzhai Road, Hefei 230026, China
[b] Institute of Sustainable Energy Technology, Department of Architecture and Built Environment, University of Nottingham, University Park, Nottingham NG7 2RD, UK

ARTICLE INFO

ABSTRACT

This paper presents an experimental and analytical study on incorporation of thermoelectric modules with glass evacuated-tube heat-pipe solar collectors. The integrated solar heat-pipe/thermoelectric module (SHP-TE) can be used for combined water heating and electricity generation. The experimental prototype unit comprises a glass evacuated-tube, a heat-pipe and a thermoelectric module with its one side attached to the condensation section of the heat-pipe and other side attached to a water channel. The heat-pipe transfers the solar heat absorbed within the glass evacuated-tube to the thermoelectric module. Under the condition of given solar irradiation and water temperature, the current, voltage and power outputs of the thermoelectric module are given for variable external electrical resistance. An analytical model of the prototype unit is presented to relate its thermal and electrical efficiencies with the solar irradiation, ambient temperature, water temperature, areas of the glass evacuated-tube and the thermoelectric module, and the length, cross-section area and number of thermoelements in the thermoelectric module. The analytic model is validated against the experimental data before it is used to optimize the design and operating parameters of the prototype for combined water heating and additional electricity generation.

1. Introduction

The pressing issue of the diminishing reserve of fossil fuels and environmental pollution caused by its combustion has stimulated the fast growth of the solar water heating market at an average annual growth rate of about 30%. China is in a leading position in production and installation of solar water heating systems. By 2006, the annual production of solar collectors had exceeded 20 million m² and the total installation had reached 90 million m² [1]. Thanks to its feature of high efficiency and anti-freezing, the evacuated-tube solar collector has become the most popular design for solar water heating in the past decades. The evacuated-tube solar collectors currently take more than 80% of solar water heating market [1]. The glass evacuated-tube solar collectors have better thermal efficiencies at the higher temperature than the conventional flat-plate solar collectors and they are suitable for applications at the temperature of above 80 °C [2]. Zambolin and Del Col [3] have experimentally compared the evacuated-tube and flat-plate solar collectors. The efficiency curve of the evacuated-tube solar collector was much flatter than the flat-plate solar collector. The average water temperature at the crossover point of the two efficiency curves is 46.6 °C for the solar irradiance of 700 W/m² and the ambient temperature of 20 °C. When the average water temperature is increased from 50 °C to 90 °C, the thermal efficiency of the evacuated-tube solar collector decreases from about 60% to 50% [4]. On the other hand, the water temperature is usually required in the range of 35–50 °C for domestic hot water or space heating [4]. These imply that with a small expense of its thermal efficiency, an evacuated-tube solar collector may be used at a higher temperature to drive a combined water heating and power generation. One attractive option is to incorporate the evacuated-tube solar collectors with thermoelectric modules to produce additional electricity besides its hot water production. Compared with solar heat driven mechanical power generation, thermoelectric modules are much more suitable for small-scale applications as they are reliable, light and compact, and have no mechanical moving parts. They are also friendly to the environment as no working fluid is used.

Though the relatively low conversion efficiency is a drawback, there has been still a growing interest recently to use thermoelectric modules for electricity generation from waste heat of

* Corresponding author. Tel.: +86 551 3607390; fax: +86 551 3606459.
E-mail address: hwei@ustc.edu.cn (W. He).

various sources when the reliability and compactness are the main consideration [5–8]. Research on system optimization and performance improvement of thermoelectric generators (TEG) for waste heat recovery has been reported in a number of publications [9–13]. In a study, the cost of electricity produced by TEG from waste warm water is predicted to be £ 0.08/kWh and even to be £ 0.04/kWh, which can challenge the cost of electricity produced by conventional methods from fossil fuels [12]. On the other hand, solar heat driven TEG is emerging as a competing alternative technology to the dominating solar photovoltaic (PV) systems. Though as its low conversion efficiency compared to PV, solar-driven TEG technology still attracts increasing attention as other simple and competitive way to produce electricity from solar energy [14–18]. In fact, the low conversion efficiency may be not a serious barrier for use of the free and friendly solar energy. With the decreasing price of thermoelement materials, the solar heat driven TEG technology would become more attractive. The performance of the TEG in a hybrid PV-TEG system, where the TEG operates independently as a secondary generator to improve the overall efficiency of the system, has been studied [18,19]. Typically, the thermal conductivity of a TEG is about 1.5 W/mK and the depth of commercial TEG is about 4 mm (including the ceramic electric insulation), so the heat flux through a TEG could be higher than 20000 W/m^2 for a temperature difference of 60–100 K. However, the solar irradiation is usually less than 1000 W/m^2, which is obviously too low to match the required heat flux of a TEG to obtain a sufficient temperature difference for a considerable efficiency. Circulation of a heat transfer medium such as water or oil is a simple way to accumulate the collected solar heat and deliver it at a high heat flux to match the operation of a TEG. Solar concentration represents another ways to obtain a high flux of solar heat for operation of a TEG. Some researchers have investigated use of a line-focus parabolic trough (PTC), a Compound Parabolic Concentrator (CPC) or a two-stage concentrator to provide high density of solar radiation so as to give a high heat flux across the TEG [15–17]. However, A CPC usually has a concentration ratio of less than 5, which is still too low to match the required heat flux of a TEG, so it needs to be used along with a circulation system. Solar tracking parabolic concentrators can easily give a much larger concentration ratio, but the cost of a tracking system could be a barrier. Use of a liquid circulation system to transfer solar heat to a TEG is simple, but a larger temperature change of the liquid is required to carry a certain amount of heat, and electricity consumption of the circulation pump and heat loss of the circulation system are other concerns.

Direct incorporation of a thermoelectric module with a heat-pipe type evacuated-tube solar collector may offer an attractive design to overcome the drawbacks of using a water circulation system. In fact, converting low heat flux to high heat flux is the one of main functions of a heat-pipe by changing the ratio of evaporator area to condenser area at an almost constant temperature. Therefore, this paper will investigate incorporation thermoelectric modules with evacuated-tube heat-pipe solar collectors for combined water heating and additional electricity generation. Design, testing and performance analysis of a prototype system will be presented.

2. Mathematical model

Incorporation a thermoelectric module with a glass evacuated-tube heat-pipe solar collector is shown in Fig. 1. An integrated solar heat-pipe/thermoelectric module (SHP-TE) consists of a glass evacuated-tube, a heat-pipe with heat transfer fin and a thermoelectric module. The A–A cross-sectional view shows the details of the thermoelectric module and the condenser section of the heat-pipe. A copper plate is soldered to the condenser of the heat-pipe in
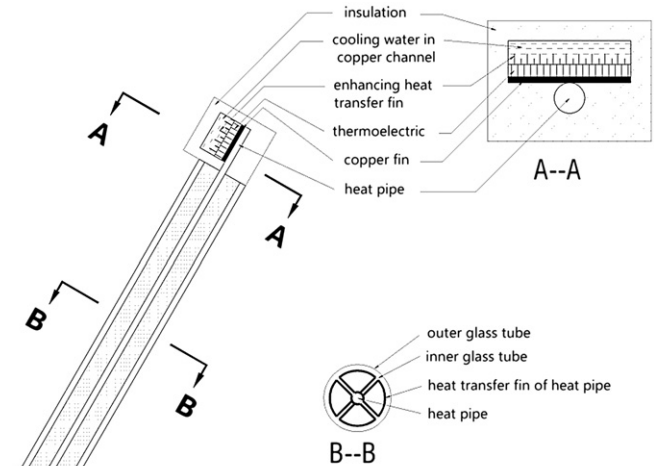

Fig. 1. The schematic diagram of an integrated SHP-TE system.

order to enhance heat transfer, and the thermoelectric module may be bonded to the copper plate tightly using silicon grease. The B–B cross-sectional view shows the detailed structure of the double-skin glass evacuated-tube with the heat-pipe being inserted. The evacuated space is between the inner glass tube and the outer glass tube. Attached to the inside surface of the inner glass tube is a thin copper cylinder with a cross fin which is in a close contact with the heat-pipe. Solar radiation is absorbed on the coated copper cylinder and solar heat is transferred to the heat-pipe through the cross fin. This design configuration has become popular because it provides an assembling convenience. The heat-pipe has a much shorter condenser section than its evaporator section, so the heat flux is much higher at the condenser section. It was intended that the mathematical model would be used to analyze the steady state performance of the incorporated system, so the following assumptions were made to simplify analysis of the complex heat transfer process in the SHP-TE:

1) The temperature gradient axially and longitudinally across the fin and the wall of the heat-pipe is neglected, so they have a uniform temperature, i.e., the lumped capacitance model applies.
2) The contact thermal resistance and electric resistance between any two parts of the system are neglected.
3) The water jacket containing the condenser section of the heat-pipe and the thermoelectric module is well insulated without any heat loss to the surroundings.
4) All the energy balance equations are for the steady state conditions, so the thermal capacity of any parts of the SHP-TEG system is neglected.
5) The SHP-TEG system operates under constant solar radiation.
6) The square of external electrical resistance is assumed to equal the product of internal electrical resistance and external electrical resistance, i.e., $R_{load}^2 = R_{te}R_{load}$.

2.1. Heat balance of the outer glass tube

The heat balance of the outer tube of the double-skin glass evacuated-tube may be given by:

$$h_{o-tube,amb}(T_{o-tube} - T_{amb}) + h_{o-tube,sky}(T_{o-tubeo} - T_{sky})$$
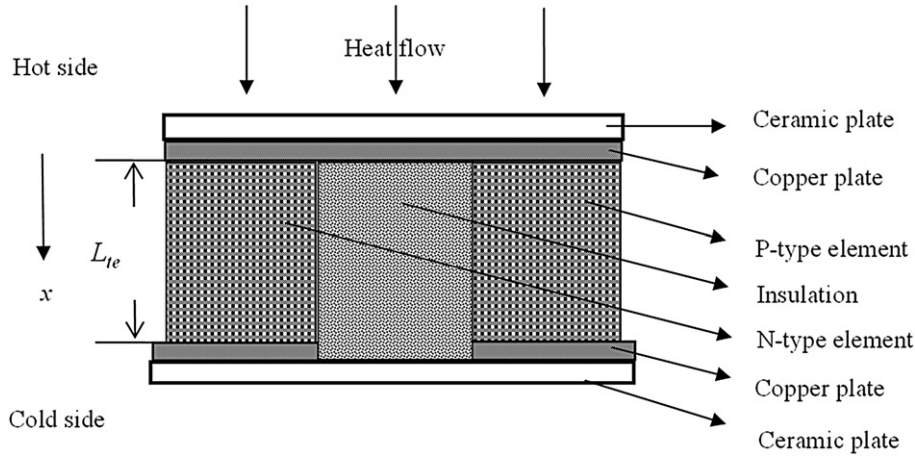$$= h_{o-tube,i-tubei}A_{i-tube}(T_{i-tube} - T_{o-tube}) \qquad (1)$$

Fig. 2. Schematic view of a thermoelectric element.

where T_{o-tube}, T_{i-tube}, T_{amb} and T_{sky} are the temperatures of the outer and inner glass tubes, the ambient temperature and the sky temperature, respectively.

The convective heat transfer coefficient between the outer glass tube and the ambient, which may be given by: $h_{o-tube,amb} = 3.8 + 2.7$ (wind speed).

The radative heat transfer coefficient between the outer glass tube and the sky, which may be given by: $h_{o-tube,sky} = \varepsilon_{o-tube}\delta(T_{sky}^2 + T_{o-tube}^2)(T_{sky} + T_{o-tube})$.

The convective heat transfer coefficient between the outer and inner glass tubes may be given by:

$$h_{o-tube,i-tube} = \delta\left(T_{o-tube}^2 + T_{i-tube}^2\right)(T_{o-tube} + T_{i-tube})/\left[1/\varepsilon_{i-tube}\right.$$
$$\left. +\frac{A_{o-tube}}{A_{i-tube}}(1/\varepsilon_{o-tube} - 1)\right].$$

where δ is the Stefan–Boltzmann constant; ε_{o-tube} and ε_{i-tube} are the emissivity of the outer glass tube and inner glass tube, A_{o-tube} and A_{i-tube} are the surface areas of the outer glass tube and the inner glass tube.

2.2. Heat balance of the inner glass tube and heat-pipe

It was not the intention of this study to analyze the detailed heat transfer through the inner glass tube, the heat-pipe and its cross fin, so they were treated as a lumped thermal capacitance, that is, they have a uniform temperature and thus $T_{i-tube} = T_{hp}$. The heat balance for the inner glass tube and heat-pipe under the steady state condition may be given by:

$$G\tau_{o-tube}\alpha_{i-tube}A_{abs} = h_{o-tube,i-tube}A_{i-tube}(T_{hp} - T_{o-tube})$$
$$+ h_{hp,te-h}A_{te}(T_{hp} - T_{te-h}) \quad (2)$$

where G is the global solar irradiance, τ_{o-tube} is the transmissivity of the outer glass tube, α_{i-tube} is the equivalent absorptivity of the inner glass tube and heat-pipe, A_{abs} is the effective solar absorption area, T_{hp} is the temperature of the heat-pipe, A_{te} is the area of the thermoelectric module, T_{te-h} is the temperature of the hot side of the thermoelectric module and $h_{hp,te-h}$ is the equivalent heat transfer coefficient between the heat-pipe and the hot side of the thermoelectric module.

2.3. Energy balance of the thermoelectric module

Fig. 2 shows one thermoelement consisting of a P-type semiconductor element, a N-type semiconductor element and a thermal insulation between the copper plates. The differentiating energy balance equation for the thermoelement is:

$$j_{te}^2 \rho_{te} + k_{te}\frac{d^2T_{te}}{dx^2} = 0 \quad (3)$$
$$T_{te}|_{x=L_{te}} = T_{te-c}; \quad T_{te}|_{x=0} = T_{te-h}$$

where j_{te} and ρ_{te} are electric current density and electric resistivity respectively.

Integrating Eq. (3) gives the temperature distribution across the thermoelement along the x axis:

$$T(x) = T_{te-h} - \frac{x}{L_{te}}(T_{te-h} - T_{te-c}) - \frac{\rho_{te}j_{te}^2}{2k_{te}}x(x - L_{te}) \quad (4)$$

Therefore, the heat flux on the hot side and cold side of the thermoelement can be obtained:

$$-k_{te}\frac{dT(x)}{dx}\bigg|_{x=0} = \frac{k_{te}}{L_{te}}(T_{te-h} - T_{te-c}) - \frac{\rho_{te}j_{te}^2}{2k_{te}}L_{te} \quad (5)$$

$$-k_{te}\frac{dT(x)}{dx}\bigg|_{x=L_{te}} = \frac{k_{te}}{L_{te}}(T_{te-h} - T_{te-c}) + \frac{\rho_{te}j_{te}^2}{2k_{te}}L_{te} \quad (6)$$

The heat balance at the hot side and cold side of the thermoelement may be described as below considering heat transfer through the insulation.

At the hot side:

$$h_{hp,te-h}A_{te-h}(T_{hp} - T_{te-h}) = S_{P-te}T_{te-h}j_{te}A_{te,P}$$
$$- k_{te}A_{P-te}\frac{dT(x)}{dx}\bigg|_{x=0} - S_{N-te}T_{te-h}j_{te}A_{N-te}$$
$$- k_{te}A_{N-te}\frac{dT(x)}{dx}\bigg|_{x=0} + k_{ins}A_{ins}\frac{T_{te-h} - T_{te-c}}{L_{te}} \quad (7)$$

At the cold side:

$$h_{te-c,water}A_{te-c}(T_{te-c} - T_{water}) = S_{P-te}T_{te-c}j_{te}A_{P-te}$$
$$- k_{te}A_{P-te}\frac{dT(x)}{dx}\bigg|_{x=L_{te}} - S_{N-te}T_{te-c}j_{te}A_{N-te}$$
$$- k_{te}A_{N-te}\frac{dT(x)}{dx}\bigg|_{x=L_{te}} + k_{ins}A_{ins}\frac{T_{te-h} - T_{te-c}}{L_{te}} \quad (8)$$

where S_{P-te} and S_{N-te} are the Seebeck coefficients of the P-type and N-type semiconductor elements, $h_{te-c,water}$ is the convective heat transfer coefficient at the cold side of the thermoelectric module.

As $I = j_{P-te}a_{P-te} = -j_{N-te}a_{N-te}$, $A_{P-te} = n_{te}a_{P-te}$, $A_{N-te} = n_{te}a_{N-te}$ and $\Delta S = S_{P-te} - S_{N-te}$, the energy balance at the hot side and cold side can be rewritten as:

$$
h_{hp,te-h}A_{te-h}(T_{hp} - T_{te-h}) = n_{te}\Delta ST_{te-h}I - \frac{n_{te}a_{P-te}k_{P-te}}{L_{te}}(T_{te-h} - T_{te-c}) - \frac{n_{te}a_{N-te}k_{N-te}}{L_{te}}(T_{te-h} - T_{te-c}) + k_{ins}A_{ins}\frac{T_{te-h} - T_{te-c}}{L_{te}} \quad (9)
$$

$$
h_{te-c,water}A_{te-c}(T_{te-c} - T_{water}) = n_{te}\Delta ST_{te-c}I - \frac{n_{te}a_{P-te}k_{P-te}}{L_{te}}(T_{te-h} - T_{te-c}) - \frac{n_{te}a_{N-te}k_{N-te}}{L_{te}}(T_{te-h} - T_{te-c}) + k_{ins}A_{ins}\frac{T_{te-h} - T_{te-c}}{L_{te}} \quad (10)
$$

where n_{te} is the number of thermoelements, a_{P-te} is the cross-sectional area of thermoelement.

2.4. Thermal efficiency

$$
\eta_{thermal} = \frac{h_{te-c,water}A(T_{te-c} - T_{water})}{GA_{abs}} \quad (11)
$$

2.5. Load resistance for the maximum power output

The load resistance required to obtain the maximum power output under a constant solar irradiation G may be different from that for the condition of a constant temperature different between the hot side and cold side of thermoelectric module ΔT. This may be demonstrated as follows.

Open circuit voltage of a thermoelectric module is:

$$
U = n_{te}(S_{P-te} - S_{N-te})(T_{te-h} - T_{te-c}) = n_{te}\Delta S\Delta T \quad (12)
$$

Electrical power output:

$$
P = U^2 R_{load} \Big/ \left[R_{load} + n_{te}\left(\frac{\rho_{N-te}L_{te}}{a_{N-te}} + \frac{\rho_{P-te}L_{te}}{a_{P-te}}\right) \right]^2
$$
$$
= U^2 R_{load} / (R_{load} + R_{te})^2 \quad (13)
$$

$\Delta T = T_{te-h} - T_{te-c}$ and the internal resistance of the thermoelectric module is $R_{te} = n_{te}(\rho_{N-te}L_{te}/a_{N-te} + \rho_{P-te}L_{te}/a_{P-te})$.

Substituting Eq. (12) into Eq. (13) gives:

$$
P = \frac{(n_{te}\Delta S\Delta T)^2 R_{load}}{(R_{load} + R_{te})^2} \quad (14)
$$

For the condition of constant solar irradiation G, ΔT varies with R_{load}, then differentiating Eq. (14) gives:

$$
\frac{dP}{dR_{load}} = \frac{(n_{te}\Delta S)^2 R_{load}}{(R_{load} + R_{te})^2}\frac{d(\Delta T^2)}{dR_{load}} + \frac{(n_{te}\Delta S)^2 \Delta T^2}{(R_{load} + R_{te})}
$$
$$
- 2\frac{(n_{te}\Delta S)^2 \Delta T^2 R_{load}}{(R_{load} + R_{te})^3} \quad (15)
$$

which should be equal to zero in order to achieve the maximum electrical power output, that is,

$$
\frac{dP}{dR_{load}} = (n_{te}\Delta S)^2
$$
$$
\frac{\Delta T^2 R_{te} - \Delta T^2 R_{load} + 2R_{load}(R_{load} + R_{te})\Delta T\frac{d\Delta T}{dR_{load}}}{(R_{load} + R_{te})^3} = 0 \quad (16)
$$

thus,

$$
\frac{2d\Delta T}{\Delta T dR_{load}}R_{load}^2 + \left(\frac{2R_{te}d\Delta T}{\Delta T dR_{load}} - 1\right)R_{load} + R_{te} = 0 \quad (17)
$$

which is complex to get R_{load} expressed with R_{te} as variable. In order to get a simple expression of R_{load}, R_{load}^2 may be assumed to be $R_{te}R_{load}$. As there is no big difference between R_{te} and R_{load}, this assumption would not cause any significant error, so Eq. (17) can be written as:

$$
\frac{2}{\Delta T}\frac{d\Delta T}{dR_{load}}R_{te}R_{load} + \left(\frac{2R_{te}}{\Delta T}\frac{d\Delta T}{dR_{load}} - 1\right)R_{load} + R_{te} = 0 \quad (18)
$$

Rearranging Eq. (18) gives:

$$
R_{load} = \frac{R_{te}}{1 - \frac{4R_{te}}{\Delta T}\frac{d\Delta T}{dR_{load}}} \quad (19)
$$

which represents the load resistance required to obtain the maximum electrical power output. This is obviously different from the required $R_{load} = R_{te}$ for the condition of constant ΔT as well discussed in the literature.

For the constant solar irradiation, the maximum electrical power output leads to the maximum electrical generation efficiency, which is defined by:

$$
\eta_{electric} = P/(GA_{abs}) \quad (20)
$$

3. Experimental apparatus

To verify the mathematical model of the incorporated thermoelectric module and evacuated-tube heat-pipe solar collector, a prototype unit was constructed according to the schematic structure shown in Fig. 1. The photograph and schematic diagram in Fig. 3 show the test rig for the prototype unit. The glass evacuated-tube had a length of 1.8 m, the diameter of the outer glass tube was 57 mm and that of the inner glass tube was 47 mm. The inner glass tube had a coated selective film with $\alpha_{i-tube} = 0.95$. The condenser section of the heat-pipe was fixed on a thin copper plate with the thickness of 1 mm and the area of 0.04 m × 0.04 m to match the length and width of the thermoelectric module. Water was circulated over the copper plate to receive the heat rejected from the cold side of the thermoelectric module. A temperature controller was used to control the inlet water temperature within the accuracy of ±0.5 C. As there was only one evacuated-tube used, the water temperature different between the inlet and outlet of the water jacket attached on a single thermoelectric module was too small to be recorded, so it was impossible to determine the thermal performance of the prototype unit. However, its electrical performance could be readily to measure. A variable electrical resistor shown in Fig. 3(b) was used to give different value of the load resistance, at which the voltage and current output were measured. Meanwhile, the global solar irradiation on a tilted surface where
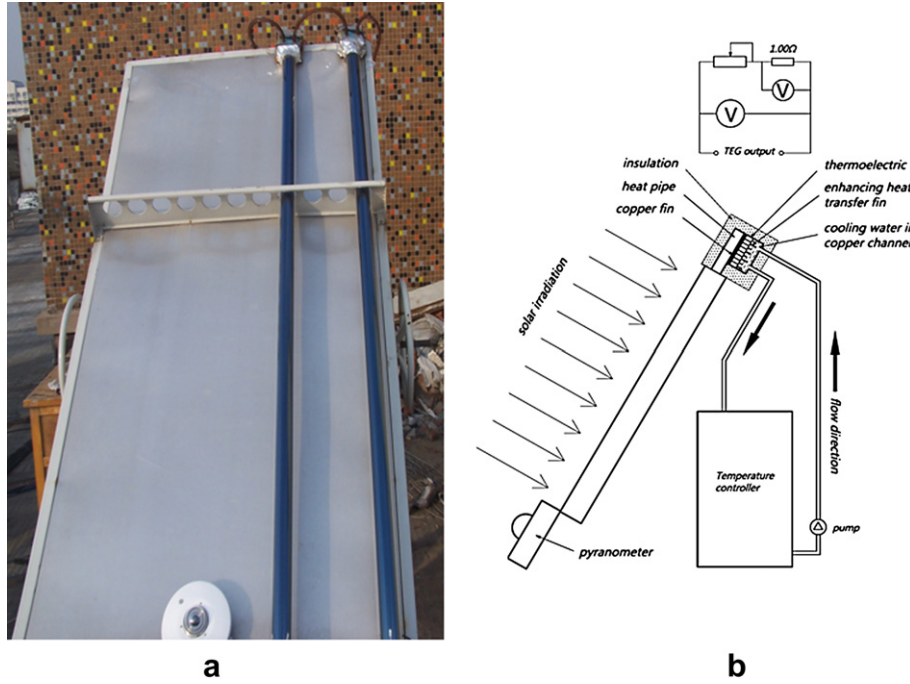
Fig. 3. Photograph and schematic diagram of the experimental apparatus.

the prototype unit was fixed was recorded, so the electrical efficiency of the prototype unit could be determined.

A commercially available Bi_2Te_3 based thermoelectric module with a size 40 mm × 40 mm × 4.0 mm and a matrix of $n_{te} = 127$ thermoelements which had a length $L_{te} = 1.5$ mm. The overall thickness of ceramic and copper plates was 2.5 mm. The cross-sectional area a_{P-te} and a_{N-te} of thermoelectric element was 1.4 mm × 1.4 mm. The main thermoelectric properties of the module were measured by the manufacturer at room temperature. The the appropriately averaged Seebeck coefficient, electrical resistance and thermal conductivity are $S_{P-te} = -S_{N-te} = 2.0 \times 10^{-4}$ V/K; $\rho_{P-te} = \rho_{N-te} = 1.0 \times 10^{-5} \Omega m$; $k_{te} = 1.5$ W/mK; $k_{ins} = 0.04$W/mK; $n_{te}\Delta S = 0.05$ V/K, $R_{te} = 2.6\Omega$, $K_{te} = 0.6$ W/K.

Fig. 4 shows the experimental results of voltage, current and electrical power output under the condition of water temperature 30 °C and solar irradiation 850 ± 20 W/m^2. It can be seen that the electrical power output P changes with R_{load} and reach the maximum value of about 0.98 W at the load resistance $R_{load} = 3.7\Omega$, which is about 1.42 times R_{te} but not equal to R_{te} as explained by Eq. (19). When R_{load} increases further, P becomes smaller but does not change much. The simulation based on the mathematical model described in Section 2 was also carried out for the same condition as the experiment and the simulation results are given along with the experimental data in Fig. 4. It is evident that they show a good agreement. Fig. 5 shows the experimental data of voltage, current and electrical power output and their comparison with the simulation for the water temperature of 40 °C and solar irradiation of 780 ± 15 W/m^2. The maximum power output was obtained when R_{load} was also about 3.7Ω. It means that higher water temperature
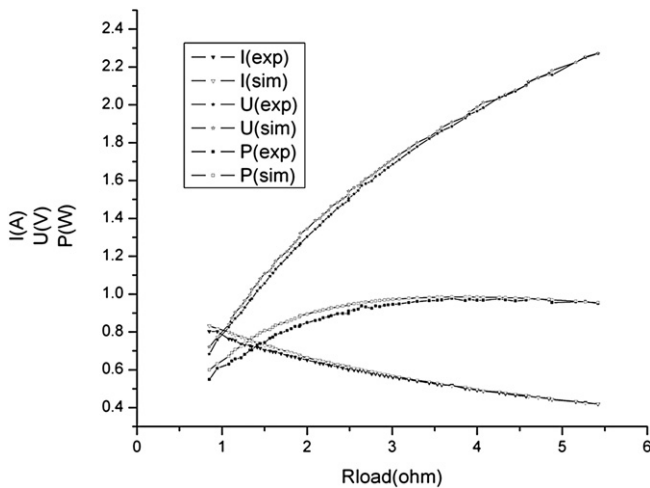

Fig. 4. Variations of voltage, current and electrical power (water temperature 30 °C, solar irradiation 850 ± 20 W/m^2).
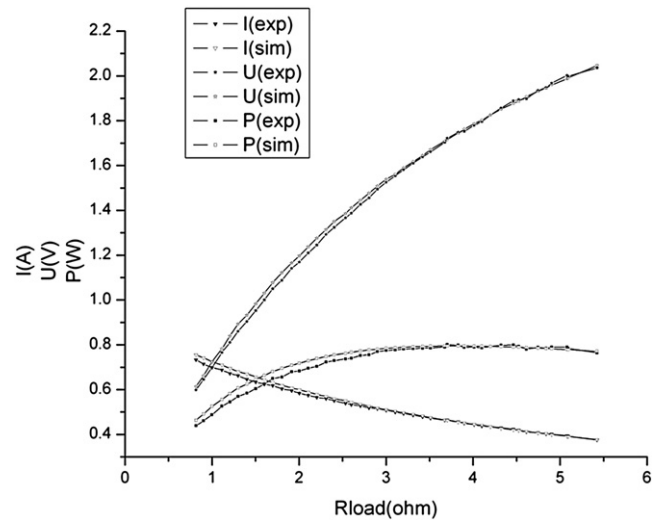

Fig. 5. Variations of voltage, current and electrical power (water temperature 40 °C, solar irradiation 780 ± 15 W/m^2).

with lower solar irradiation may change the maximum electrical power output but the selection of R_{load} varied little. A good agreement between the experiment and simulation can also be seen in Fig. 5, the maximum difference is less than 10%.

4. Parametric analysis

After the mathematical model had been verified by the experimental data of the prototype unit, the simulation was carried out to study the parametric effect on the thermal and electric efficiencies of the prototype SHP-TE unit. The parameters described in Section 3 were used as the base case.

4.1. Water temperature

Fig. 6 shows the change of the simulated thermal efficiency and electrical efficiency with water temperature for the solar irradiation of 1000 W/m² and the ambient temperature of 25 °C. Both thermal efficiency and electrical efficiency of the SHP-TE unit decrease with increasing water temperature. When the water temperature varies from 25 °C to 55 °C, the electrical efficiency is decreased from 1.625% to 1.255% while the thermal efficiency is decreased from 59.36% to 52.96%. The thermal efficiency of solar heat-pipe without TE is also shown in Fig. 6, which varies from 80.15% to 75.46%. There is about 20−25% thermal energy reduction which is converted into electrical power by TE.

4.2. Solar irradiation

Fig. 7 shows the simulation results of thermal efficiency and electrical efficiency at the water temperature of 45 °C for different solar irradiations. It is clear that the electric efficiency of the SHP-TE unit increases with increasing solar irradiation. This means that the surface temperature of the heat-pipe increases with the solar irradiation, so the heat loss to the ambient will increase. When the solar irradiation is lower, increasing it may have larger effect on the thermal efficiency than the increasing heat loss and power output, so the thermal efficiency increases with the solar irradiation. But, when the solar irradiation is larger, the increasing power output and heat loss may have larger effect, hence the thermal efficiency decreases with increasing solar irradiation. Therefore, the thermal efficiency of the SHP-TE unit exhibits the maximum value of 56.65% at the solar irradiation of 500 W/m² for the condition of simulation.
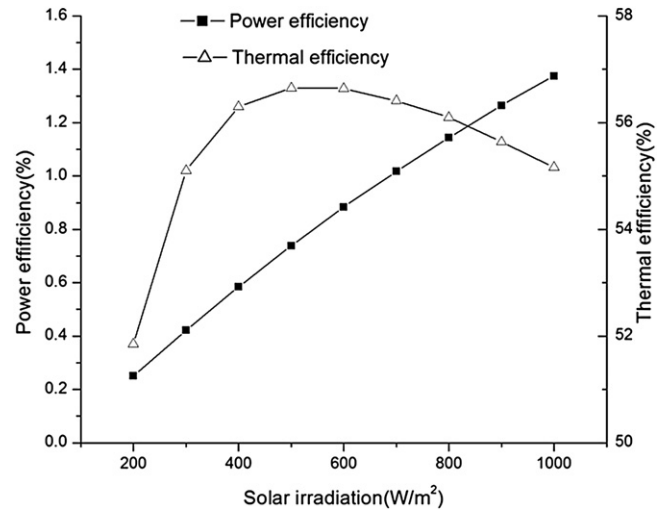

Fig. 7. Thermal and electrical efficiencies vary with solar irradiation.

4.3. Number of thermoelements

The change of the simulated thermal efficiency and electrical efficiency at the water temperature of 45 °C with the number of thermoelements is shown in Fig. 8. It is obvious that there is a maximum point for electrical efficiency when the number of thermoelements varies. According to Eq. (12),fewer number of thermoelements in a thermoelectric module causes lower voltage and thus lower electric output if the ΔT is constant. But, with the number of thermoelements increasing, the area of insulation as seen in Fig. 2 decreases, so the heat conduction between the hot side and cold side of the thermoelectric module increases. This may lead to a smaller ΔT and thus a lower voltage and power output. Therefore, there is a maximum electrical efficiency with increasing the number of thermoelements. Fig. 8 shows that the optimal number of thermocelement increases from 50 to 80 with increasing solar irradiation from 400 W/m² to 1000 W/m².

It can also be seen from Fig. 8 that the thermal efficiency of the SHP-TE unit always increases with the number of thermoelements. This is because increasing the number of thermoelements causes increased heat conduction through the thermoelectric module,
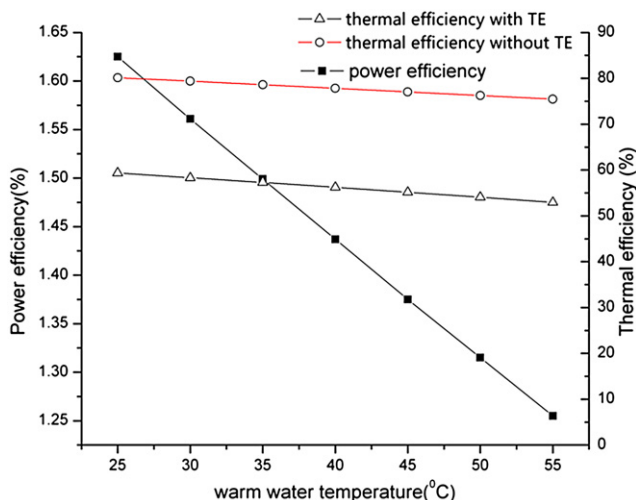

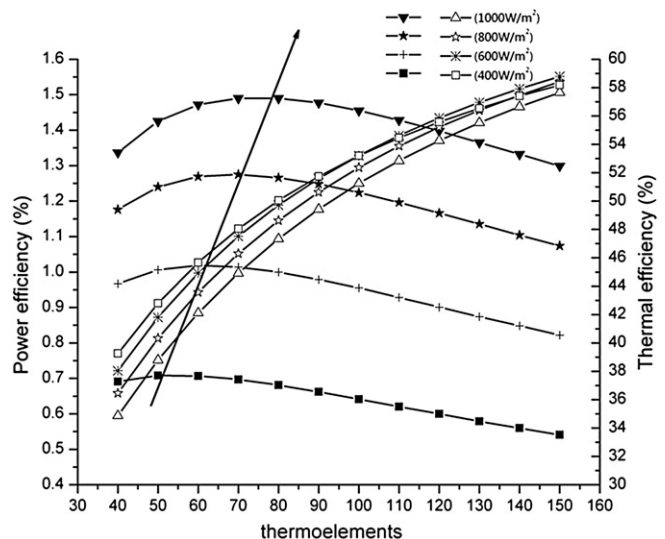Fig. 6. Thermal and electrical efficiencies vary with water temperature.

Fig. 8. Thermal and electrical efficiencies vary with the number of thermoelements.
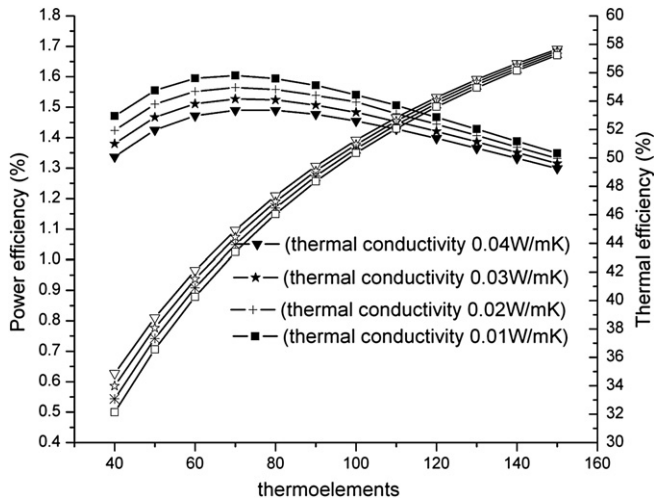
Fig. 9. Thermal and electrical efficiencies vary with the number of thermoelements for various values of thermal conductivity of insulation.

thus the thermal efficiency increases while the electrical efficiency decreases.

4.4. Thermal conductivity of insulation

Fig. 9 shows the effect of thermal conductivity of insulation between the hot side and cold side of the thermoelectric module for the condition of solar irradiation 1000 W/m^2 and water temperature 45 °C. As expected, a good thermal insulation leads to a higher electrical efficiency and lower thermal efficiency. It can also be seen that the effect of thermal insulation becomes smaller with increasing the number of thermoelements.

5. Conclusions

Incorporation of thermoelectric modules with glass evacuated-tube heat-pipe solar collectors has been studied through simulation and experiment. The integrated solar heat-pipe/thermoelectric module (SHP-TE) can be used for combined water heating and electricity generation. A mathematical model of the SHP-TE unit has been presented to predict the thermal and electrical performance of the SHP-TE for given solar irradiation, ambient and water temperatures, geometrical and thermoelectric parameters. The external load resistance required for the maximum power output under the constant solar irradiation has been derived. The optimum load resistance is different from that for the condition of constant temperature difference across a thermoelectric module. An experimental apparatus has been set up to provide data for verification of the mathematical model. It has been seen a good agreement between the simulation results and experimental data. The verified mathematical model has been used to simulate the effect of design and operation parameters on the thermal and electrical efficiencies of the SHP-TE unit. The simulation results indicate that for the water temperature of 45 °C and the solar irradiation of larger than 600 W/m^2 the SHP-TE unit may have a thermal efficiency of about 55% and meanwhile have an electrical efficiency above 1%.

Compared with an organic Rankine cycle system with about 3–4% electrical efficiency [20], the SHP-TE system has 1–2% electrical efficiency which is a little lower than an organic Rankine cycle system, but the SHP-TE system is simple, and hasn't any movement components and it is easy to replace any units of SHP-TE system.

Nomenclature

T	temperature, °C
h	convective or radiative heat transfer coefficient, W/m^2
δ	the Stefan–Boltzmann constant
ε	emissivity
A	surface area, m^2
G	global solar irradiance, W/m^2
τ	transmissivity
α	absorptivity
j	electric current density, A/m^2
ρ	electric resistivity, Ωm
k	thermal conductivity, W/mK
L	thickness of a thermoelectric module, m
x	thickness variable, m
S	Seebeck coefficient, V/K
a	cross-sectional area of semiconductor thermoelement, m^2
n	number of thermoelements in a thermoelectric module
R	electrical resistance, Ω
U	voltage, Volt
I	current, A
p	power, Watt
$\eta_{thermal}$	thermal efficiency
$\eta_{electric}$	electrical efficiency

Subscripts

$o-tube$	outer glass tube in a double-skin glass evacuated-tube
$i-tube$	inner glass tube in a double-skin glass evacuated-tube
sky	sky
amb	ambient
abs	solar absorption
hp	heat-pipe
te	thermoelectric module
$te-h$	hot side of a thermoelectric module
$te-c$	cold side of a thermoelectric module
$water$	cooling water
$P-te$	P-type semiconductor thermoelement
$N-te$	N-type semiconductor thermoelement
$load$	external electrical resistance

References

[1] Wang RZ, Zhai XQ. Development of solar thermal technologies in China. Energy November 2010;35(11):4407–16.

[2] Tang Runsheng, Gao Wenfeng, Yu Yamei, Chen Hua. Optimal tilt-angles of all-glass evacuated tube solar collectors. Energy September 2009;34(9):1387–95.

[3] Kim Yong, Seo Taebeom. Thermal performances comparisons of the glass evacuated tube solar collectors with shapes of absorber tube. Renewable Energy April 2007;32(5):772–95.

[4] Zambolin E, Del Col D. Experimental analysis of thermal performance of flat plate and evacuated tube solar collectors in stationary standard and daily conditions. Solar Energy August 2010;84(8):1382–96.

[5] Ma Liangdong, Lu Zhen, Zhang Jili, Liang Ruobing. Thermal performance analysis of the glass evacuated tube solar collector with U-tube. Building and Environment September 2010;45(9):1959–67.

[6] Douglas Crane T, Gregory Jackson S. Optimization of cross flow heat exchangers for thermoelectric waste heat recovery. Energy Conversion and Management 2004;45:1565–82.

[7] Champier D, Bedecarrats JP, Rivaletto M, Strub F. Thermoelectric power generation from biomass cook stoves. Energy 2010;35:935–42.

[8] Niu Xing, Yu Jianlin, Wang Shuzhong. Experimental study on low-temperature waste heat thermoelectric generator. Journal of Power Sources 2009;188:621–6.

[9] Gou Xiaolong, Xiao Heng, Yang Suwen. Modeling, experimental study and optimization on low-temperature waste heat thermoelectric generator system. Applied Energy 2010;87:3131–6.

[10] Stevens James W. Optimal design of small ΔT thermoelectric generation systems. Energy Conversion and Management 2001;42:709–20.

[11] Chen Lingen, Gong Jianzheng, Sun Fengrui, Wu Chih. Effect of heat transfer on the performance of thermoelectric generators. International Journal of Thermal Sciences 2002;41:95–9.

[12] Rowe DM, Min Gao. Evaluation of thermoelectric modules for power generation. Journal of Power Sources 1998;73:193–8.

[13] Yu Jianlin, Zhao Hua. A numerical model for thermoelectric generator with the parallel-plate heat exchanger. Journal of Power Sources 2007;172:428–34.

[14] Chen Lingen, Li Jun, Sun Fengrui, Wu Chih. Performance optimization of a two-stage semiconductor thermoelectric-generator. Applied Energy 2005; 82:300–12.

[15] Siddig Omer A, David Infield G. Design and thermal analysis of a two stage solar concentrator for combined heat and thermoelectric power generation. Energy Conversion & Management 2000;41:737–56.

[16] Xi Hongxia, Luo Lingai, Fraisse Gilles. Development and applications of solar-based thermoelectric technologies. Renewable and Sustainable Energy Reviews 2007;11:923–36.

[17] Omer SA, Infield DG. Design optimization of thermoelectric devices for solar power generation. Solar Energy Materials and Solar Cells 1998;53: 67–82.

[18] Rockendorf Gunter, Sillmann Roland, Podlowski Lars, Litzenburger Bernd. PV-Hybrid and thermoelectric collectors. Solar Energy 1999;67(4–6): 227–37.

[19] Vorobiev Yu, Gonzalez-Hernandez J, Vorobiev P, Bulat L. Thermal-photovoltaic solar hybrid system for efficient solar energy conversion. Solar Energy 2006; 80:170–6.

[20] Wang XD, Zhao L, Wang JL, Zhang WZ, Zhao XZ, Wu W. Experimental investigation on the low-temperature solar Rankine cycle system using R245fa. Energy Conversion and Management 2011;52:946–52.